Published OnlineFirst September 20, 2019; DOI: 10.1158/1541-7786.MCR-19-0243

Cell Fate Decisions

Molecular Cancer Research

The Zinc-Finger AN1-Type Domain 2a Gene Acts as a Regulator of Cell Survival in Human Melanoma: Role of E3-Ligase cIAP2

Sofia Pizzato Scomazzon[1], Anna Riccio[1,2], Silvia Santopolo[1], Giulia Lanzilli[2], Marta Coccia[1,2], Antonio Rossi[2], and M. Gabriella Santoro[1,2]

Abstract

The zinc-finger AN1-type domain-2a gene, also known as AIRAP (arsenite-inducible RNA-associated protein), was initially described as an arsenite-inducible gene in *Caenorhabditis elegans* and mammalian cells. Differently from the AIRAP worm homologue, *aip-1*, a gene known to play an important role in preserving animal lifespan and buffering arsenic-induced proteotoxicity, mammals have a second, constitutively expressed, AIRAP-like gene (AIRAPL), recently implicated in myeloid transformation. We have identified human AIRAP as a canonical heat-shock gene, whose expression, differently from AIRAPL, is strictly dependent on the proteotoxic-stress regulator heat-shock factor 1 (HSF1). AIRAP function is still not well defined and there is no information on AIRAP in cancer. Herein we show that bortezomib and next-generation proteasome inhibitors ixazomib and carfilzomib markedly induce AIRAP expression in human melanoma at concentrations comparable to plasma-levels in treated patients. AIRAP-downregulation leads to bortezomib sensitization, whereas AIRAP-overexpression protects melanoma cells from the drug, identifying AIRAP as a novel HSF1-regulated marker of chemotherapy resistance. More importantly, this study unexpectedly revealed that, also in the absence of drugs, AIRAP-silencing hinders melanoma clonogenic potential and spheroid growth, promoting caspase activation and apoptotic cell death, an effect independent of AIRAPL and linked to downregulation of the antiapoptotic protein cIAP2. Interestingly, AIRAP was found to interact with cIAP2, regulating its stability in melanoma. Taken together, the results identify AIRAP as a novel HSF1-dependent regulator of prosurvival networks in melanoma cells, opening new therapeutic perspectives in chemoresistant melanoma treatment.

Implications: The findings identify ZFAND2A/AIRAP as a novel stress-regulated survival factor implicated in the stabilization of the antiapoptotic protein cIAP2 and as a new potential therapeutic target in melanoma.

Introduction

The zinc-finger AN1-type domain-2a (ZFAND2A) gene, also known as AIRAP (arsenite-inducible RNA-associated protein), was initially described as a highly conserved gene encoding an inducible cysteine- and histidine-rich 19-kDa protein, whose expression can be activated by arsenite and electrophiles in *Caenorhabditis elegans* and mammalian cells (1, 2). AIRAP, and its worm homologue, *aip-1*, were suggested to interact with the proteasome's 19S regulatory cap, adapting the cell core protein degradation machinery to counteract proteotoxicity induced by arsenite or other environmental toxins (2). Mammals have a second AIRAP-like gene (AIRAPL/ZFAND2B), which is constitutively expressed and also encodes a proteasome-interacting protein (3). The fact that in worms a single gene, *aip-1*, incorporates features of both the arsenic-inducible AIRAP and the constitutively expressed AIRAPL has suggested that AIRAP and AIRAPL represent a relatively late feature of evolution apparently restricted to mammals (3). We have previously demonstrated that in humans AIRAP behaves as a canonical heat-shock gene, whose expression, differently from AIRAPL, is temperature-dependent and strictly controlled by the proteotoxic-stress regulator heat-shock factor 1 (HSF1; ref. 4).

The human genome encodes 6 HSFs: HSF1, HSF2, HSF4, HSF5, HSFX, and HSFY that have different functions and exhibit different and tissue-specific patterns of expression; among these HSF1 is considered the paralog responsible for regulating stress-induced transcriptional responses (5). HSF1 is generally found as an inert monomer in unstressed cells; upon exposure to proteotoxic stress, HSF1 is derepressed in a stepwise process that involves trimerization, nuclear translocation, phosphorylation/sumoylation, and binding to DNA sequences (heat-shock elements, HSE), characterized by inverted repeats of a "nGAAn"-pentameric motif (6). HSF1-binding to HSE triggers a rapid shift in the transcriptional program resulting in the expression of cytoprotective heat-shock proteins (HSP), which include molecular chaperones of the HSP70 family and other proteins of the network (6). In human cells, HSF1-binding sites have been described also in genes

[1]Department of Biology, University of Rome Tor Vergata, Rome, Italy. [2]Institute of Translational Pharmacology, CNR, Rome, Italy.

Note: Supplementary data for this article are available at Molecular Cancer Research Online (http://mcr.aacrjournals.org/).

S. Pizzato Scomazzon and A. Riccio contributed equally to this article.

Current address for S. Pizzato Scomazzon: School of Health Sciences, Pontifícia Universidade Católica do Rio Grande do Sul, Porto Alegre, Brazil.

Corresponding Author: M. Gabriella Santoro, University of Rome Tor Vergata, Via della Ricerca Scientifica, Rome 00133, Italy. Phone: 39-06-72594822; Fax: 39-06-72594821; E-mail: santoro@uniroma2.it

Mol Cancer Res 2019;17:2444–56

doi: 10.1158/1541-7786.MCR-19-0243

Published OnlineFirst September 20, 2019; DOI: 10.1158/1541-7786.MCR-19-0243

encoding proteins with non-chaperone function (7–9). We have identified in the human AIRAP promoter a specific HSE-sequence located at position -211 to -202 from the transcription start site that is responsible for HSF1-binding and transcriptional activation (4). We have also shown that AIRAP expression is potently induced, via HSF1, by bortezomib (Velcade, formerly PS-341; ref. 10), a 26S-proteasome inhibitor (PI) used in the clinic for treatment of multiple myeloma and showing anticancer activity against several other malignancies, including melanoma, based on its direct pro-apoptotic effects on cancer cells and its anti-angiogenic action (11–13). Interestingly, bortezomib potently induces AIRAP transcription at concentrations comparable to plasma-levels in treated patients (10).

Although it was found to associate with the proteasome 19S-cap (2–3), AIRAP function is still not well defined; in particular, whereas AIRAPL was recently involved in myeloid transformation (14), there is no information on AIRAP function in cancer cells. We therefore investigated the role of AIRAP in the anticancer activity of bortezomib. In an initial screening we found that the PI strikingly induced AIRAP expression in human melanoma cells at nanomolar concentrations. Melanoma was then selected for this study, also based on the known anticancer activity of bortezomib against this type of malignancy (13, 15).

Herein we report that AIRAP downregulation leads to bortezomib sensitization in melanoma cells, whereas AIRAP overexpression partially protects melanoma cells from bortezomib-induced apoptosis. Surprisingly we found that, also in the absence of pro-apoptotic stimuli, AIRAP-silencing resulted in hindering tumor clonogenic potential and spheroid growth; moreover we show that AIRAP-downregulation promotes destabilization of the antiapoptotic protein cIAP2 and triggers caspase-dependent apoptosis in melanoma cells.

Materials and Methods

Cell culture, treatments, plasmids, and transfections

Human malignant melanoma cell lines M10 (kindly provided by G. Zupi; ref. 16), SK-MEL-28, SK-MEL-5, WM115, and A375 (ATCC) were authenticated by STR-profiling and tested for mycoplasma contamination. Cells were maintained in RPMI1640 media containing 10% of FCS, 2 mmol/L glutamine and antibiotics. Cell viability was determined by vital-dye exclusion assay (Trypan blue, 0.1%) and MTT assay (10). Bortezomib, ixazomib-citrate, carfilzomib (Selleckchem), and MG132 (AdipoGen) were dissolved in dimethylsulfoxide (DMSO) and diluted in culture medium; control media contained the same amount of DMSO-vehicle (<0.1%). TNFα (Peprotech) and cycloheximide (MyBioSource) were dissolved in water. The cFlag-tagged AIRAP-pcDNA3 vector (AIRAP-Flag) was described previously (4). To generate the cFlag-tagged AIRAP-pBABE vector, the human *AIRAP* gene was amplified from ZFAND2A cDNA clone ID-5263788 (Open Biosystems) using the following primers: 5′-GGCGGATCCACCATGGAGTTTCCTGATTTGGGGAAG-3′ and 5′-TGCGGTCGACCCTACTTATCGTCGTCATCCTTGTAATCCCCAGCTTTGATGGTGGGGCG-3′. The PCR product was digested with *Bam*H1 and *Sal*1, and inserted into a *Bam*H1/*Sal*1-cut pBABE vector; construct nucleotide-sequence was verified by DNA-sequencing. The pCMV3-Myc-cIAP2/BIRC3 (cIAP2-Myc) vector was obtained by Sino-Biological. Transfections were performed using jetPRIME Transfection-Reagent (Polyplus-transfection), according to the manufacturer's instructions.

Recombinant retroviral vectors and generation of AIRAP-expressing melanoma cells

Retroviruses were produced by 293T cell transfection with plasmids expressing retroviral proteins Gag-Pol, G (VSV-G pseudotype), pBABE, and cFlag-tagged AIRAP-pBABE constructs using Lipofectamine-2000 (Invitrogen). Supernatants containing retroviral particles were collected 48 hours after transfection. M10 cells were infected in the presence of 8 μg/mL polybrene overnight, and cells containing pBABE and cFlag-tagged AIRAP-pBABE constructs were selected with puromycin (1 μg/mL) 48 hours after infection. After 10 days in selective medium, 2 pools [cFlag-tagged AIRAP-pBABE (M10-AIRAP) and M10-pBABE] were isolated. Puromycin was removed 24 hours before experimental procedures.

siRNA interference

Three siRNA duplex sequences (siAIRAP1, siAIRAP2, and siAIRAP3) and their scrambled control (scRNA; Qiagen) were used for AIRAP-silencing (Supplementary Table S1). Transfections were performed using jetPRIME Transfection-Reagent. Briefly, cells were plated on 35 mm wells (4×10^5 cells/well) and, after 24 hours, were transfected with 50 nmol/L of the indicated siRNAs, siRNA pools (25 nmol/L siAIRAP1 and 25 nmol/L siAIRAP2) or scRNA. siRNAs were left in the medium for the duration of the experiment unless differently specified. For bortezomib-treatment experiments, siRNAs were removed 24 hours after transfection and cells were washed with culture medium before treatment.

Western blot and immunoprecipitation

Whole-cell extracts (WCE) were prepared in high-salt extraction buffer-B, as described (17). Equal amounts of protein (20 or 30 μg/sample) were separated by SDS-PAGE and blotted to nitrocellulose. Primary and secondary-peroxidase-labeled antibodies used are listed in Supplementary Table S2. Detection was performed using the Super-Signal Detection Kit (Pierce). For immunoprecipitation (IP), WCE (200 μg) were precleared at 4°C for 1 hour with protein-A agarose-beads (40 μL; Roche) in buffer-B and incubated overnight with anti-AIRAP antibodies (2 μg/200 μg cell lysate), followed by a 2-hour incubation at 4°C with protein A-agarose beads. After extensive washing, immunocomplexes were analyzed by Western blot (WB). WCE aliquots (25 μg) were used as input. For cross-linking experiments, M10 cells were cotransfected with AIRAP-Flag and cIAP2-Myc expression-vectors and, after 24 hours, were fixed with formaldehyde (1% final concentration; Sigma) for 5 minutes; the reaction was quenched adding glycine (125 mmol/L, pH 8). After extensive washing in W-solution (50 mmol/L Tris-HCl pH 7.4, NaCl 150 mmol/L), cells were lysed in 300 μL RIPA-buffer containing protease inhibitors, sonicated on ice using Sonics Vibra-Cell VCX (21% amplitude, pulse-mode: 12 × 10s, 15s-pauses) and centrifuged at 15.000 × *g* (10 minutes). Lysates (500 μg) were incubated overnight at 4°C with anti-Flag (2 μg) or anti-cIAP2 (2 μg) antibodies and packed protein G-agarose (25 μL; Roche). Beads were washed with RIPA-buffer, and then incubated at 95°C with SDS-reducing-buffer (62.5 mmol/L Tris-HCl pH 6.8, 20% glycerol, 2% SDS, 5% β-mercaptoethanol) to revert cross-linking. Quantitative evaluation of proteins was determined by Versadoc-1000 (Bio-Rad) using Quantity-One software-program (Bio-Rad). PARP–cPARP ratios were determined after normalization of PARP and cPARP to β-actin levels in the same sample.

Published OnlineFirst September 20, 2019; DOI: 10.1158/1541-7786.MCR-19-0243

Electrophoretic mobility shift assay

Whole cell extracts (15 μg protein/sample) were incubated with a [^{32}P]-labeled HSE DNA-probe followed by analysis of DNA-binding activity by electrophoretic mobility shift assay (EMSA). Binding reactions were performed as described (18). Complexes were analyzed by nondenaturing 4% PAGE.

qRT-PCR analysis

Total RNA was prepared using TRizol (Invitrogen) according to the manufacturer's protocol. Samples (1 μg RNA) were reverse transcribed as described (4). qRT-PCR analyses were performed with specific primers, listed in Supplementary Table S1, using SsoAdvanced-Universal-SYBR-Green Supermix (CFX96; Bio-Rad). Relative quantities of selected mRNAs were normalized to β-actin.

Clonogenic assay

Cells transfected for 24 hours with siAIRAP or scRNA were washed with culture medium and treated with bortezomib or vehicle. After 24 and 48 hours, equal number of viable cells were plated (400 cells/35 mm-well) and incubated at 37°C for 10 days. Adherent cells were fixed with 4% paraformaldehyde for 10 minutes and stained with 0.1% crystal-violet. Colonies with more than 50 cells were considered positive. Surviving fraction was calculated as described (19).

Quantitative assessment of cell death and apoptosis

Cell death was assessed by trypan-blue exclusion. Apoptosis was evaluated by FACScan flow-cytometry using AnnexinV-FITC/propidium iodide staining according to the manufacturer's protocol (FITC-AnnexinV Apoptosis-Detection Kit; Becton-Dickinson). Data were processed by CellQuest-software program (Becton-Dickinson). Nuclear fragmentation in AIRAP-silenced cells was detected by confocal microscopy after 4′,6-diamidino-2-phenylindole (DAPI; Sigma-Aldrich) staining.

Confocal microscopy

Cells grown on coverslips and treated with bortezomib for 14 hours were fixed with 4% paraformaldehyde and permeabilized with PBS-TRITON 0.2%. After incubation with a blocking-solution containing 10% normal goat serum-3% BSA for 1 hour, cells were incubated with anti-AIRAP antibodies (Sigma-Aldrich) for 1 hour followed by decoration with TRITC-conjugated anti-rabbit IgG. Nuclei were stained with DAPI. Images (800 × 800 pixels resolution) were captured using Olympus-Fluoview-FV1000 confocal laser scanning-system (Olympus America) and analyzed using Imaris-6.2 software (Bitplane). Images shown in all figures are representative of at least 5 random fields.

Proximity ligation assay

Cells were grown on coverslips and processed as described previously; after incubation with primary antibodies, Duolink *in situ* Proximity ligation assay (PLA; Sigma-Aldrich) was performed as described previously (9). Briefly, PLA probes were incubated for 1 hour at 37°C, followed by hybridization, ligation (30 minutes at 37°C) and amplification (100 minutes at 37°C). Nuclei were stained with DAPI in Duolink In-Situ Mounting-Medium (Sigma-Aldrich). Antibodies used are: anti-AIRAP, anti-Flag, and anti-cIAP2 (Supplementary Table S2). Confocal microscopy was performed as described previously.

3D melanoma spheroid formation and growth

M10 and SK-MEL-28 cells were transfected with siAIRAP (siRNA pools: 25 nmol/L siAIRAP1 and 25 nmol/L siAIRAP2) or scRNA and, after 72 hours, equal number of viable cells (2×10^4/well) were seeded in round-bottomed, ultra-low attachment 96-well spheroid microplates (Corning) in 200 μL RPMI1640 medium supplemented with 10% FCS and antibiotics. Spheroids (at least 6 per condition) were grown at 37°C for 10 days in the absence of siRNAs. Compact spheroids formed 24 hours (M10) or 72 hours (SK-MEL-28) after cell seeding. Spheroid size and morphology were analyzed with a Leica DM-IL microscope equipped with a 5× objective and images were captured on a Leica-DC300 camera using Leica-IM500 software. Spheroid area was measured using ImageJ software (20). 3D-spheroid models were generated using ReViSP (MatLab-software) to analyze differences in size and shape (21). Spheroid volume was calculated with ReViSP (21).

Statistical analysis

Statistical analysis was performed using the Student *t* test for unpaired data (Prism 5.0 software; GraphPad). Data are expressed as the mean ± SD, and *P* values <0.05 were considered significant. All the results shown are representative of at least 3 independent experiments in duplicate.

Results

The anticancer drug bortezomib potently induces AIRAP expression in melanoma cells

Bortezomib was recently shown to induce AIRAP expression via HSF1 in human endothelial cells (10). To investigate the effect of bortezomib (Fig. 1A) on AIRAP expression in human melanoma, M10 cells derived from metastatic melanoma nodules (16) were treated with different concentrations of bortezomib and, after 24 hours, WCE were analyzed by Western blot for levels of AIRAP, the chaperone HSP70 as a marker of HSF1-activation, and poly-ubiquitinated proteins and caspase-3 substrate PARP as control of bortezomib activity. As shown in Fig. 1B, bortezomib-treatment causes a dose-dependent accumulation of polyubiquitinated proteins and HSP70, as well as PARP-cleavage, which was evident at concentrations above 5 nmol/L. Low levels of AIRAP were detected in untreated M10 cells, whereas a dose-dependent increase in AIRAP level was evident in bortezomib-treated cells. In addition to bortezomib, elevated AIRAP levels were detected in M10 cells treated with MG132 and next-generation PIs ixazomib and carfilzomib (Supplementary Fig. S1); also in this case, AIRAP induction was associated with HSP70 expression.

In addition to M10 cells, bortezomib-treatment also resulted in a large increase in AIRAP levels in different human melanoma cell lines, including SK-MEL-28, SK-MEL-5, and WM115 cells (Fig. 1C).

To investigate the kinetics of AIRAP expression, M10 monolayers were treated with 25 nmol/L bortezomib and, at different times after treatment, WCE were analyzed for levels of polyubiquitinated proteins, AIRAP, HSP70, and PARP by WB, as well as for HSF1 DNA-binding activity levels by EMSA. In parallel samples, total RNA was analyzed for levels of AIRAP and HSP70 mRNA by qRT-PCR. As shown in Fig. 1D, bortezomib treatment causes polyubiquitinated proteins

Published OnlineFirst September 20, 2019; DOI: 10.1158/1541-7786.MCR-19-0243

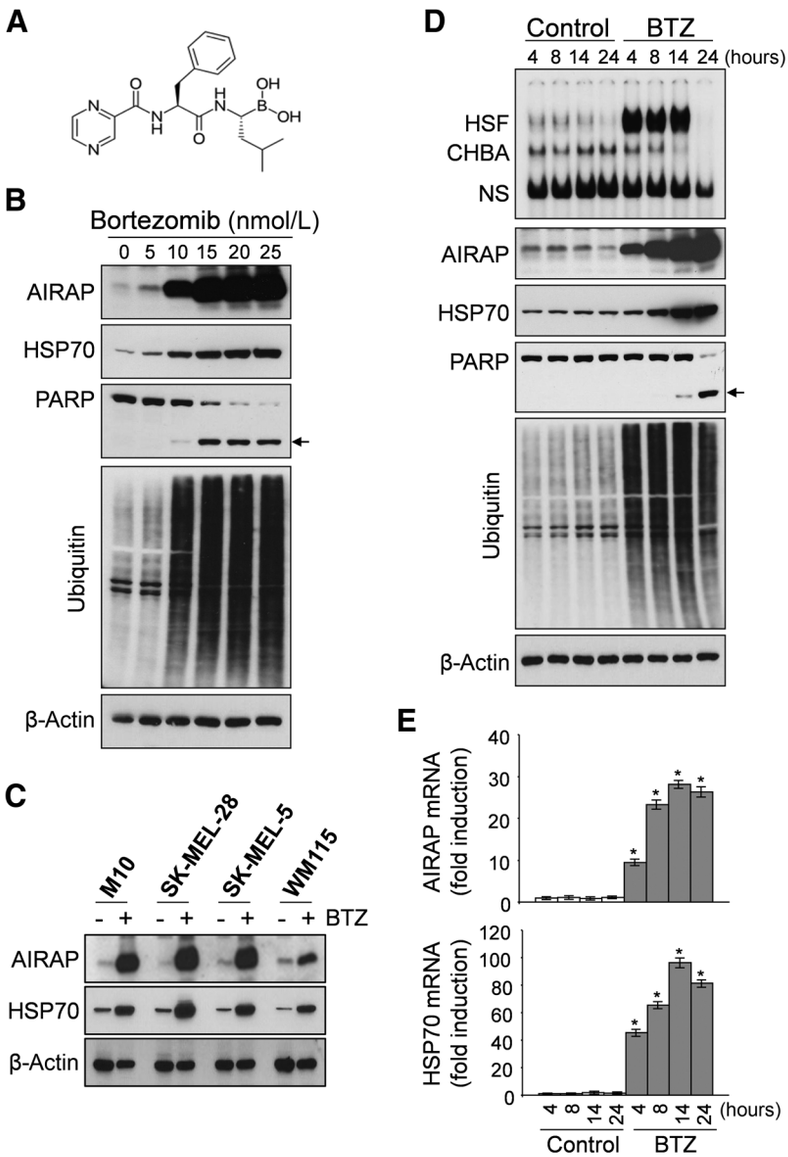

Figure 1.

Bortezomib potently induces AIRAP expression in melanoma cells. **A,** Structure of bortezomib (BTZ). **B,** Levels of AIRAP, HSP70, PARP, ubiquitin and β-actin were determined by Western-blot (WB) in M10 cells treated with different concentrations of bortezomib for 24 h. **C,** M10, SK-MEL-28, SK-MEL-5 and WM115 melanoma cells were treated with 20 nmol/L BTZ (+) or vehicle (−) and, after 48 hours, WCE were analyzed for levels of AIRAP, HSP70, and β-actin by WB. **D,** M10 cells were treated with 25 nmol/L BTZ or vehicle (Control) and, at different times, WCE were analyzed for HSF1 DNA-binding activity by EMSA (top) and for levels of AIRAP, HSP70, PARP, ubiquitin, and β-actin by WB (bottom). Positions of the HSF DNA-binding complex (HSF), constitutive HSE-binding activity (CHBA) and nonspecific protein–DNA interaction (NS) are shown. **E,** In parallel samples, total RNA was analyzed for AIRAP, HSP70, and β-actin expression by qRT-PCR. Relative quantities of AIRAP and HSP70 RNAs were normalized to β-actin. Fold increase was calculated by comparing the induction of the indicated genes in the treated samples to the relative control, which was arbitrarily set to 1. All reactions were made in duplicate using samples derived from at least 3 biological repeats. Error bars indicate ± SD. *, $P < 0.05$.

accumulation in M10 cells starting at 4 hours after treatment. Parallel with polyubiquitinated proteins accumulation, bortezomib triggers HSF1 DNA-binding activity (Fig. 1D), and induces AIRAP-mRNA expression starting at 4 hours of treatment and reaching maximal levels between 14 and 24 hours with a kinetics similar to HSP70-mRNA (Fig. 1E). Concomitantly, high levels of AIRAP protein were found to accumulate in bortezomib-treated cells up to 24 hours after treatment (Fig. 1D).

To characterize bortezomib-induced AIRAP intracellular localization, M10 cells growing on coverslips were treated with bortezomib and after 14 hours were examined by confocal-immunomicroscopy. An intense AIRAP immunofluorescent signal was found to be distributed throughout the cytoplasm, and partially in the nucleus in bortezomib-treated cells (Supplementary Fig. S2). AIRAP nuclear and cytoplasmic distribution is consistent with previous observations in different human cell types (10).

AIRAP modulates bortezomib anticancer activity in M10 melanoma cells

The rapid and remarkable increase in AIRAP levels after bortezomib treatment prompted us to investigate the effect of AIRAP-silencing on the anticancer activity of the drug in melanoma cells. M10 cells were transiently transfected with 3 different AIRAP-siRNA (siAIRAP1, 2, and 3) or scramble-RNA (scRNA); AIRAP mRNA and protein levels were determined at 60 hours after transfection. The performance of each of the single siRNAs as well as the pools of 2 siRNAs was compared to select the best conditions for AIRAP-silencing. All 3 siRNAs were able to inhibit AIRAP expression; an optimal inhibition was obtained using the pool of siAIRAP1 and 2 (Supplementary Fig. S3A). This pool (siAIRAP) was then used for the following experiments, unless differently specified. An efficient AIRAP-silencing by siAIRAP was confirmed by IP of endogenous AIRAP in M10 cells, as well as in M10 cells overexpressing a Flag-tagged AIRAP (Supplementary Fig. S3B and S3C).

Published OnlineFirst September 20, 2019; DOI: 10.1158/1541-7786.MCR-19-0243

Next, M10 cells were transfected with siAIRAP or scRNA and, after 24 hours, were treated with 20 nmol/L bortezomib or vehicle. AIRAP levels were determined by WB after 24 hours of bortezomib-treatment (Fig. 2A). In parallel samples, cell viability was determined by trypan-blue staining and by clonogenic assay. Bortezomib was effective in causing an increase in cell death at 24 hours after treatment, which was significantly enhanced in AIRAP-silenced cells (Fig. 2A).

Surprisingly, AIRAP-silencing caused a significant increase in M10 cell death in the absence of the drug. More importantly, depletion of basal AIRAP by siRNA was found to be more effective than bortezomib-treatment in inhibiting M10 colony-forming ability, which was reduced by approximately 80% as compared with scRNA-transfected control (Fig. 2B). These effects were more pronounced at 48 hours after bortezomib-treatment (72 hours after AIRAP-silencing; Supplementary Fig. S4A and S4B).

Since bortezomib is known to induce apoptosis in melanoma cells (15), in parallel samples, WCE were analyzed for levels of PARP, caspase-3, caspase-7, caspase-8, and cleaved caspase-9 by WB to investigate the apoptotic signaling, and specifically the cascade of caspase activation induced by bortezomib and the effect of AIRAP-silencing. Bortezomib was found to promote cleavage of caspase-3, -7, and -9, and PARP already at 24 hours after treatment; these effects were enhanced in AIRAP-silenced cells (Fig. 2C), suggesting a cytoprotective role of AIRAP during bortezomib-treatment. Also in this case, these effects were more pronounced at 72 hours after AIRAP-silencing (Supplementary Fig. S4C).

To further investigate the role of AIRAP in melanoma sensitivity to bortezomib, M10 cells stably expressing Flag-tagged AIRAP (M10-A) and control M10 cells stably transfected with the empty vector (M10-p) were established as described in Materials and Methods. M10-A and M10-p cells were treated with 25 nmol/L bortezomib and, at 24 or 48 hours after treatment, were analyzed for cell viability and for cleavage of PARP and caspase-3. As shown in Fig. 2D–F, M10-A cells overexpressing AIRAP were found to be partially resistant to bortezomib, presenting a significant increase in cell viability, as well as a reduction in caspase-3 and PARP cleavage as compared with control M10-p cells. Altogether these data suggest that AIRAP plays an important role in protecting melanoma cells from bortezomib-induced cell death.

More interestingly, AIRAP-silencing was found to promote the cleavage of PARP and caspases-3, -7, and -9, as well as caspase-8, in the absence of the drug (Fig. 2C), suggesting that AIRAP-downregulation for 48 hours is sufficient to trigger apoptosis in M10 cells.

AIRAP downregulation induces apoptosis in human melanoma cells

Following these observations, M10 cells were transiently transfected with siAIRAP or scRNA and, after 24, 48, and 72 hours, WCE were analyzed for levels of PARP, caspase-3, caspase-7, caspase-8, and for autophagy markers LC3-I/II and p62/SQSTM1 by WB to investigate the apoptotic signaling *versus* autophagy induction in AIRAP-silenced cells. Levels of AIRAP and the AIRAP-like gene AIRAPL, shown to interfere with myeloid transformation (14), were determined as control. In parallel samples, total RNA was analyzed for levels of AIRAP and AIRAPL mRNA by qRT-PCR (Fig. 3A and B), and cell viability was determined by trypan-blue staining (Fig. 3C). The results confirm that AIRAP-silencing results in promoting the cleavage of PARP and caspases-3, -7, and -8 starting at 48 hours after silencing (Fig. 3). No significant changes in autophagy markers LC3-I/II and p62 were detected under conditions that lead to caspase activation up to 72 hours after silencing (Fig. 3B). In addition, AIRAP-silencing did not cause changes in AIRAPL mRNA and protein levels up to 72 hours after AIRAP-siRNA transfection, indicating that the effect of AIRAP on melanoma cell survival is independent of AIRAPL.

To determine whether the effects described above are specific for M10 cells or induction of cell death may represent a more general response of human melanoma cells to AIRAP-downregulation, 3 different human melanoma cell lines derived from primary tumors (SK-MEL-28 and WM115 cells) or from metastatic tissue (SK-MEL-5 cells) were transiently transfected with siAIRAP or scRNA and, after 72 hours, WCE were analyzed for PARP and AIRAP levels. Parallel samples were analyzed for AIRAP mRNA levels by qRT-PCR, and cell viability was determined by clonogenic assay. AIRAP-silencing resulted in PARP-cleavage in SK-MEL-28, SK-MEL-5, and WM115 cells (Supplementary Fig. S5A, S5C, and S5E), and greatly reduced (>80%) colony-forming ability in SK-MEL-28 and SK-MEL-5 cells (Supplementary Fig. S5B and S5D); we were unable to obtain colonies in the case of WM115 cells.

A substantial inhibition (>80%) of cell survival and colony-forming ability was also shown in highly aggressive A375 melanoma cells after transient AIRAP silencing (Supplementary Fig. S6).

Next, for quantitative assessment of the dynamics of the apoptotic process, M10 cells were transiently transfected with siAIRAP or scramble-RNA and, after 48 or 72 hours, apoptosis was evaluated by flow-cytometric analysis with AnnexinV-FITC (AV) and PI-staining. A time-dependent induction of apoptosis was confirmed, with 30% of early apoptotic cells (AV-positive and PI-negative) being detected at 48 hours after siAIRAP transfection, and more than 40% of late apoptotic cells (AV/PI-double-positive) detected at later (72 hours) times (Fig. 4A). Analysis of DNA fragmentation by confocal microscopy also confirmed apoptosis induction at 48 hours after AIRAP-silencing (Fig. 4B). In parallel samples, levels of AIRAP, caspase-3, PARP, LC3-I/II, and p62/SQSTM1 were analyzed by WB (Fig. 4C), confirming that there is no change in autophagy markers, under conditions that cause caspase cleavage and cell death.

AIRAP silencing inhibits melanoma spheroid growth

The effect of AIRAP-silencing on melanoma spheroid growth was also analyzed. M10 cells nontransfected, or transiently transfected with siAIRAP or scramble-RNA for 72 hours were grown as 3D-spheroids for 10 days, in the absence of siRNAs. As shown in Fig. 5A and B, spheroids growth was significantly reduced in AIRAP knockdown cells; scramble-RNA transfection had no effect on spheroid growth. Spheroid shape was analyzed on day 5 in 3D-spheroid models generated using ReViSP software (21). No relevant differences were observed in spheroid shape after AIRAP-silencing (Fig. 5C); spheroids volume, calculated with ReViSP software on day 5, confirmed that AIRAP-silencing greatly inhibits M10 spheroid growth (Fig. 5D). Similar results were obtained in a different melanoma cell line, SK-MEL-28 (Supplementary Fig. S7).

Published OnlineFirst September 20, 2019; DOI: 10.1158/1541-7786.MCR-19-0243

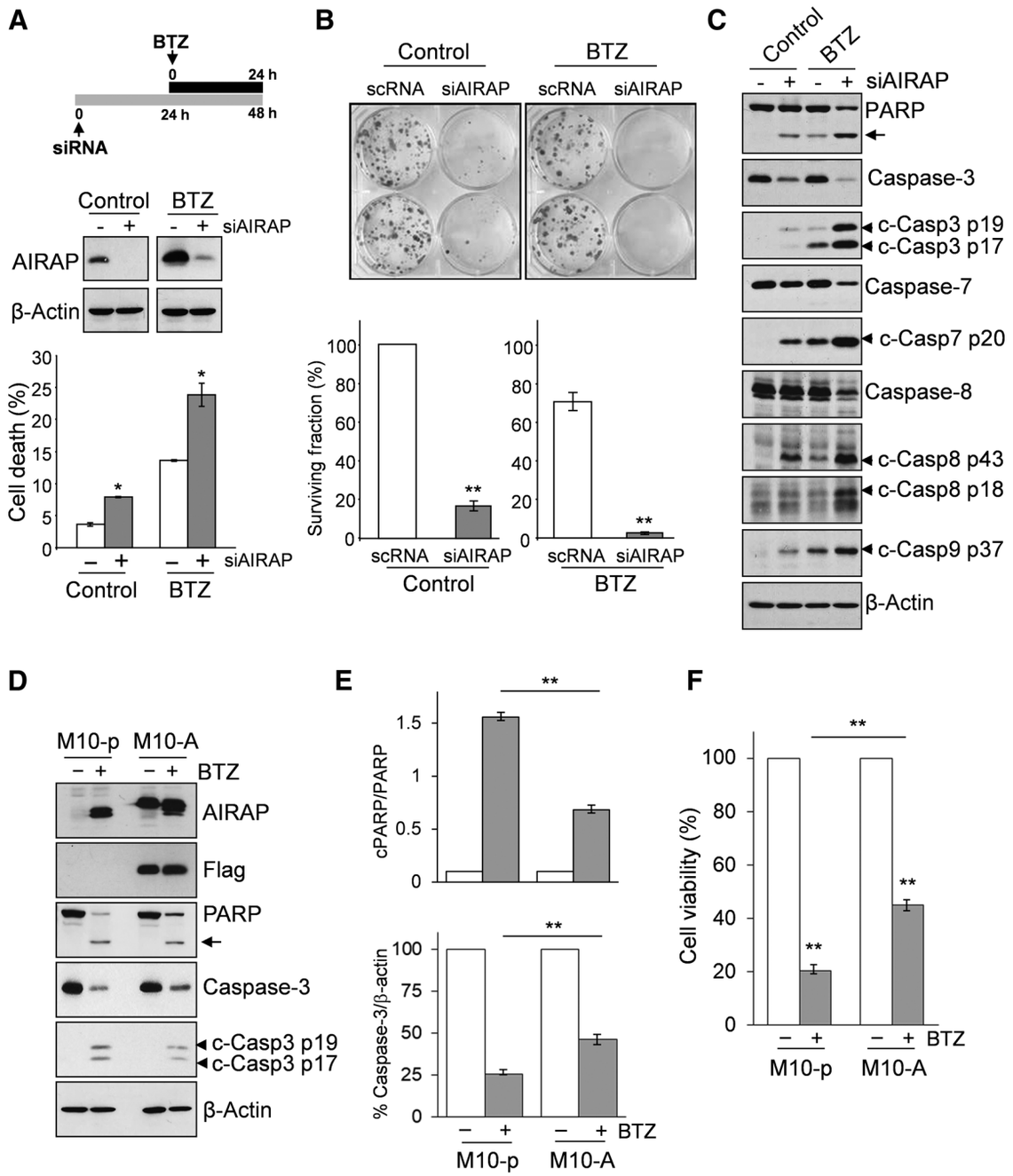

Figure 2.

AIRAP modulates bortezomib anticancer activity in melanoma cells. **A,** Schematic representation of the experimental design (top). M10 cells were transiently transfected with AIRAP-siRNA (siAIRAP) (+) or scramble-RNA (−) and, after 24 hours, were treated with 20 nmol/L bortezomib (BTZ) or vehicle (Control). After 24 hours, WCE were analyzed for levels of AIRAP and β-actin by WB (middle). In parallel samples, cell viability was determined by trypan blue staining (bottom). Error bars indicate ± SD. *, $P < 0.05$. **B,** Cell survival was analyzed in parallel samples by clonogenic assay after 10 days. Representative images (top) and quantification of clonogenic assay (bottom) are shown. Data are expressed as percentage of surviving fractions. Error bars indicate ± SD. **, $P < 0.01$. **C,** WCE of M10 cells treated as in **A** were analyzed for levels of PARP, caspase-3, caspase-7, caspase-8, cleaved caspase-9, and β-actin by WB. Full-length (caspase-3, -7, -8) and cleaved fragments (c-Casp, caspase-3, -7, -8, -9) are shown. The cleaved PARP fragment is indicated by the arrow. **D,** Control M10-pBABE (M10-p) and M10-AIRAP-Flag (M10-A) cells were treated with 25 nmol/L BTZ (+) or vehicle (−) and, after 24 hours, WCE were analyzed for levels of AIRAP, Flag, PARP, caspase-3, and β-actin by WB. Full-length and cleaved fragments of caspase-3 are shown. Arrow indicates cleaved PARP fragments. **E,** Quantification of cleaved PARP/total PARP (top) and full-length caspase-3/β-actin (bottom) of the samples shown in **D**. **F,** Cell viability of M10-p and M10-A cells treated as in **D** was determined by MTT assay at 48 hours after bortezomib-treatment. Error bars indicate ± SD. **, $P < 0.01$. **A–F,** Data from a representative experiment of 3 with similar results are shown.

Published OnlineFirst September 20, 2019; DOI: 10.1158/1541-7786.MCR-19-0243

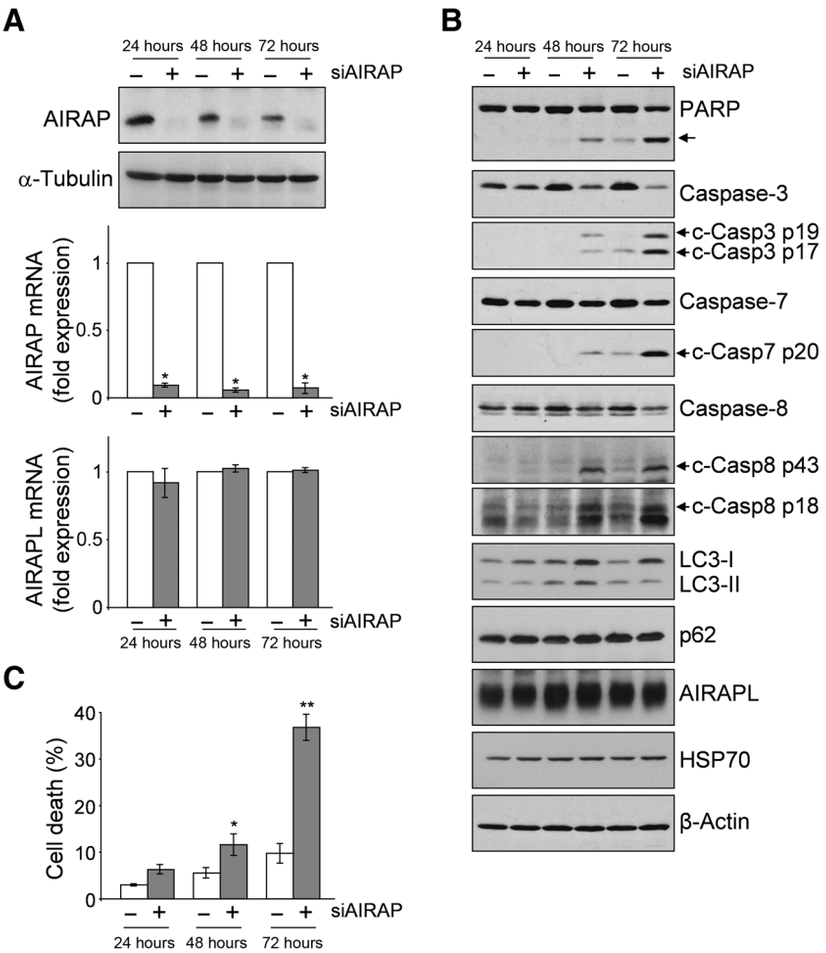

Figure 3.
AIRAP-silencing promotes PARP-cleavage without affecting AIRAPL expression. **A,** M10 cells were transfected with AIRAP-siRNA (siAIRAP) (+) or scramble-RNA (−) and, after 24, 48, and 72 hours, WCE were analyzed for levels of AIRAP and α-tubulin by WB (top). In parallel samples, total RNA was analyzed for AIRAP, AIRAPL, and β-actin expression by qRT-PCR. Relative quantities of AIRAP and AIRAPL RNAs were normalized to β-actin. Fold expression was calculated by comparing the expression of the indicated genes in silenced-samples to the relative control, which was arbitrarily set to 1. All reactions were made in duplicate using samples derived from at least 3 biological repeats. Error bars indicate ± SD. *, $P < 0.05$. **B,** In parallel samples WCE were analyzed for levels of PARP, caspase-3, caspase-7, caspase-8, LC3-I/II, p62, AIRAPL, HSP70, and β-actin by WB. Full-length (caspase-3, -7, -8) and cleaved fragments (c-Casp, caspase-3, -7, -8) are shown. Arrow indicates cleaved PARP fragments. **C,** The number of live and dead cells in parallel samples was determined by trypan blue staining. Error bars indicate ± SD. *, $P < 0.05$; **, $P < 0.01$. Data from a representative experiment of 3 with similar results are shown.

AIRAP-silencing leads to a selective reduction of cIAP2/BIRC3 protein levels in melanoma cells

Several cancers, including melanoma, are characterized by the presence of high levels of proteins that dampen pro-apoptotic signals, including members of the Bcl-2 family (Bcl-xL and A1/Bfl-1), cellular inhibitors of apoptosis (cIAP-1, cIAP-2, and XIAP), the caspase-8/FADD-like IL1β-converting enzyme (FLICE)-inhibitory protein cFLIP, and survivin, generally due to aberrant regulation of anti-apoptotic factors, including NF-κB (22). We then evaluated the effect of AIRAP-silencing on the level of several survival-regulating proteins, including cIAP-1, cIAP-2, XIAP, cFLIP, Bcl-xL, survivin, Bcl-2, as well as the melanoma-associated IAP ML-IAP/Livin, at 48 and 72 hours after transfection with siAIRAP in M10 cells. As shown in Fig. 4C, levels of cIAP2 were found to be greatly reduced already at 48 hours after AIRAP silencing, whereas no significant change was detected in the level of the other anti-apoptotic proteins examined at this time. Decreased cIAP2 levels, concomitant with PARP-cleavage, were confirmed in M10 cells silenced for AIRAP using 3 different AIRAP-siRNAs (Fig. 6A). A reduction of cIAP2, but not cIAP1, levels was detected also in SK-MEL-28 melanoma cells knockdown for AIRAP (Fig. 6B), suggesting that cIAP2 could be implicated in AIRAP-mediated regulation of melanoma cell survival. To verify this hypothesis, cIAP2 was overexpressed in control or AIRAP-silenced M10 cells using the pCMV3-Myc-cIAP2/BIRC3 construct. After 48 hours, WCE were analyzed for levels of AIRAP, Myc, cIAP2, cIAP1, and PARP by WB. As shown in Fig. 6C, AIRAP-silencing caused PARP-cleavage as expected; however, this effect was greatly reduced following cIAP2 overexpression.

AIRAP interacts with cIAP2 and is implicated in the control of cIAP2 protein stability

cIAP2 was shown to be specifically stabilized in several cancers, including melanoma, leading to resistance to pro-apoptotic stimuli (22–24). To investigate whether AIRAP-silencing leads to deregulation of cIAP2 expression or to cIAP protein degradation, M10 cells transfected with siAIRAP or scRNA for 72 hours were analyzed for levels of cIAP2 and cIAP1 proteins by WB and cIAP2 and cIAP1 mRNA by qRT-PCR. As shown in Fig. 6D, AIRAP-silencing caused a selective decrease in cIAP2 protein levels, while cIAP2 RNA levels were not significantly altered at the same time. Next, M10 cells were transiently transfected with siAIRAP or scRNA and, after 36 hours, cIAP2 expression was stimulated by TNFα (20 ng/mL). After 6 hours, samples were analyzed for AIRAP, cIAP2, and cIAP1 mRNAs and protein levels. Also in this case AIRAP-silencing caused a selective decrease in cIAP2 protein levels, whereas cIAP2 RNA levels were not reduced (Fig. 6E), confirming that AIRAP-silencing is not inhibiting cIAP2 mRNA transcription and suggesting that AIRAP may be involved in cIAP2 protein stabilization. To investigate this possibility, M10 cells

Published OnlineFirst September 20, 2019; DOI: 10.1158/1541-7786.MCR-19-0243

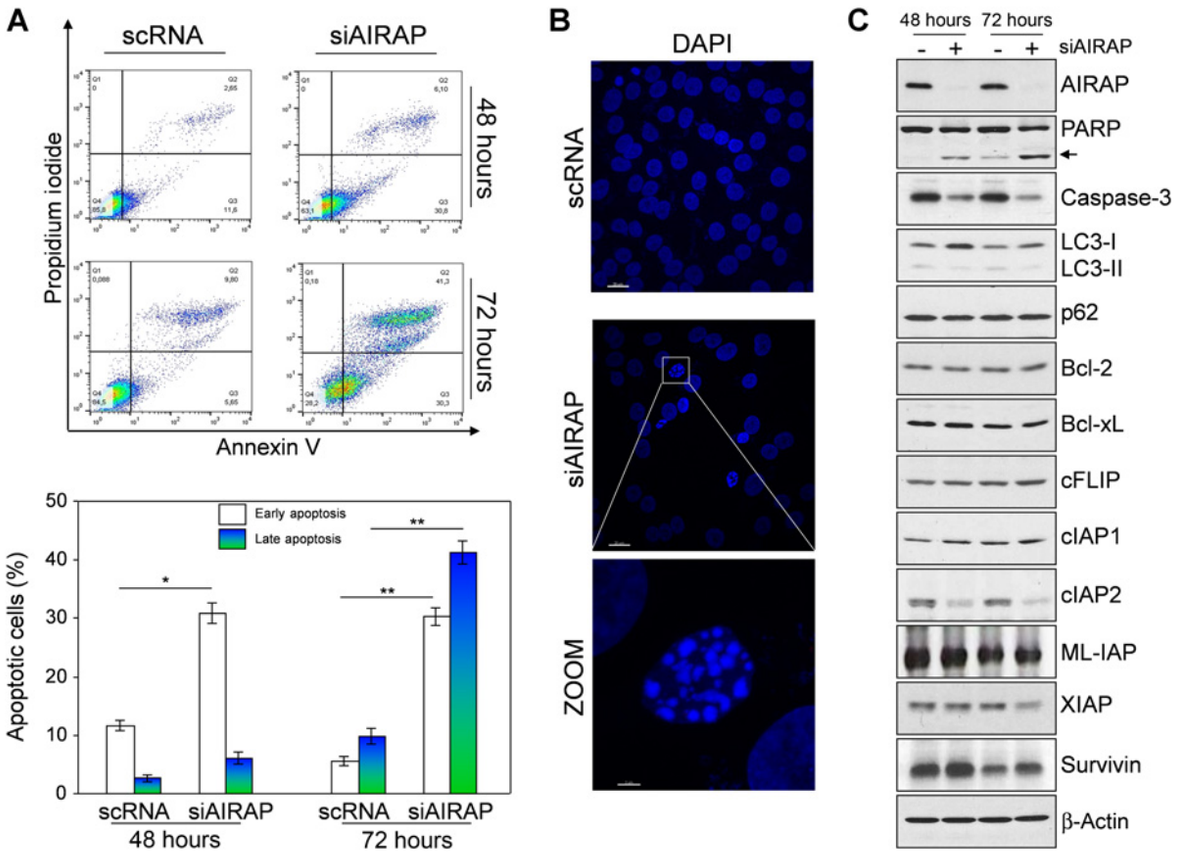

Figure 4.

AIRAP-knockdown triggers apoptosis and selectively alters cIAP2 expression in M10 melanoma cells. **A,** M10 cells were transiently transfected with AIRAP-siRNA (siAIRAP) or scramble-RNA (scRNA) and, after 48 or 72 hours, apoptosis was evaluated by flow-cytometric analysis with Annexin V-FITC and propidium iodide (PI)-staining. Data are represented by a dot-plot showing cells stained with Annexin V-FITC versus PI in a log10 scale (top). Percentages of early and late apoptotic cells are shown (bottom). Error bars indicate ± SD. *, $P < 0.05$; **, $P < 0.01$. **B,** M10 cells treated as in **A** were analyzed for DNA fragmentation after DAPI staining. Merge and zoom images are shown. Scale bar, 20 μm (zoom, 3 μm). **C,** WCE of M10 cells treated as in **A** were analyzed for levels of AIRAP, PARP, caspase-3, LC3-I/II, p62, Bcl-2, Bcl-xL, cFLIP, cIAP1, cIAP2, ML-IAP, XIAP, surviving, and β-actin by WB. Arrow indicates cleaved PARP fragments. Data from a representative experiment of 3 with similar results are shown.

were transfected with siAIRAP for 36 hours and treated with TNFα (20 ng/mL) for 4.5 hours at which time protein synthesis was arrested by adding 100 μg/mL cycloheximide. At different times after cycloheximide-treatment cIAP1, cIAP2, and α-tubulin levels were determined by WB, followed by quantitative determination by densitometric analysis. Under these conditions cIAP1 degradation was found to be minimal in both control and AIRAP-silenced cells, whereas cIAP2 half-life was significantly reduced (from 9 to 4.5 hours) in AIRAP-silenced cells as compared with control (Fig. 6F). Bortezomib treatment was not able to restore cIAP2 levels in AIRAP-silenced M10 cells (Riccio and colleagues, unpublished observation), suggesting a proteasome-independent mechanism.

The possibility that AIRAP-dependent cIAP2 stabilization in melanoma cells may rely on interaction between these 2 proteins was then investigated. AIRAP-cIAP2 colocalization was first detected by *in situ* PLA in M10 cells and in M10 cells stably expressing Flag-tagged AIRAP (Fig. 7A and B). Next, Co-IP experiments were performed in M10 cells cotransfected with AIRAP-Flag and cIAP2-myc expression vectors. At 24 hours after cotransfection, WCE were immunoprecipitated with anti-cIAP2 or anti-Flag antibodies after *in vivo* formaldehyde cross-linking. The results, shown in Fig. 7C, confirm that AIRAP interacts with cIAP2.

Discussion

The global incidence of melanoma has increased dramatically over the past few decades (25–27). Surgery is the main treatment for early-stage melanoma, whereas it is rarely curative in the advanced stages of the disease. Melanoma is usually highly resistant to conventional chemotherapy; however, in recent years, advances in the use of immunotherapy based on immune checkpoint inhibitors and in targeted therapy with the advent of *BRAF* and *MEK* inhibitors have transformed the clinical history of the disease, providing significant patient survival improvements (25–28). Despite these recent advances in chemo- and immuno-therapy, metastatic melanoma continues to represent one of the most biologically aggressive and chemoresistant

Published OnlineFirst September 20, 2019; DOI: 10.1158/1541-7786.MCR-19-0243

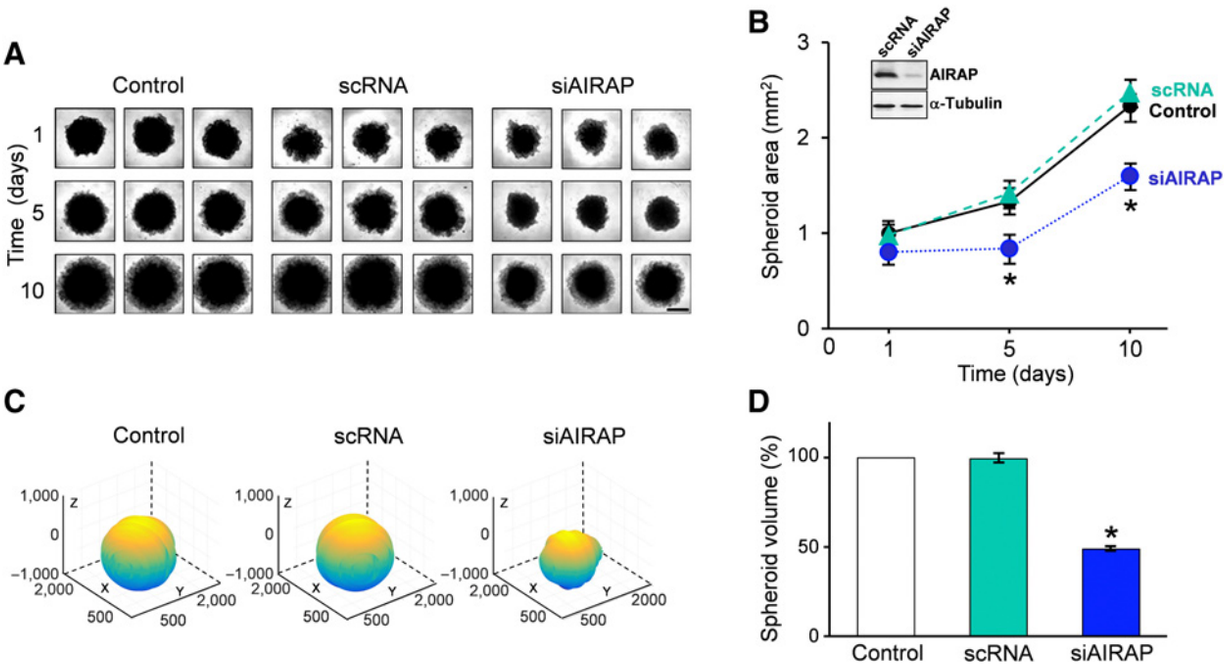

Figure 5.

AIRAP-silencing inhibits M10 melanoma spheroid growth. **A,** Bright-field images of 3 representative spheroids of mock-transfected (control), scramble-RNA (scRNA), and AIRAP-siRNA (25 nmol/L siAIRAP1 and 25 nmol/L siAIRAP2) transfected M10 melanoma cells on day 1, 5, and 10 after plating. Scale bar: 250 mm. Magnification 50×. **B,** Spheroid growth curve ($n = 6$). Error bars indicate ± SD. *, $P < 0.05$. AIRAP levels in scRNA- and siAIRAP-transfected cells at day 1 are shown (inset). **C,** ReViSP software-generated 3D models of one representative control, scRNA and siAIRAP M10 spheroid on day 5. **D,** Quantification of M10 spheroids volume, calculated with ReViSP software and expressed as percentage of control ($n = 6$). Data from a representative experiment of 2 with similar results are shown. Error bars indicate ± SD. *, $P < 0.05$.

cancers known (26, 29). The occurrence of this malignancy is known to result from the accumulation of genetic and/or epigenetic events leading to the activation of various oncogenes and to the deregulation of intracellular signaling pathways resulting in uncontrolled cell proliferation, as well as in apoptosis inhibition through upregulation of anti-apoptotic gene products, thereby causing resistance to available anticancer agents (29).

Bortezomib, a boronic acid-based PI acting on the β5-subunit of the proteasome, in current clinical use for treatment of multiple myeloma and mantle cell lymphoma (12, 30), was shown to possess anticancer activity and pro-apoptotic effects against several other malignancies, including melanoma (11–13), although, in the case of melanoma, it works most effectively in combination with other therapeutic agents (13, 31). Cancer cells counteract the pro-apoptotic effects of bortezomib through upregulation of prosurvival pathways, including the heat-shock response (HSR) via HSF1 activation (10). HSF1 orchestrates the HSR in eukaryotes, protecting healthy cells from the damaging effects of proteotoxic stress by triggering the expression of molecular chaperones (32). Cancer cells are known to boost their chaperone system to cope with stress caused by increased protein synthesis and folding, as well as proteasome overwhelming (33); therefore, cancer cells are more highly dependent on HSF1 than normal cells, presenting a "non-oncogenic" addiction to HSF1 (5, 34). In different types of cancers HSF1 levels and nuclear localization are strongly increased (35–39), and HSF1 was found to regulate a malignant-specific transcriptional program critical for cancer cells and tumor microenvironment (40); elevated nuclear HSF1 levels were also associated with poor disease outcome in cancer, including in patients with melanoma (36, 39, 41). However, the mechanisms involved in HSF1 prosurvival activity in cancer are still poorly understood.

We have recently identified AIRAP as a novel human heat-shock gene whose expression is strictly controlled by HSF1 (4, 10). Herein we show that AIRAP is implicated in the response of melanoma cells to bortezomib. In fact the PI, at concentrations comparable to plasma-levels in treated patients (10), strongly induces AIRAP expression in different types of melanoma cells; AIRAP downregulation markedly enhances bortezomib anticancer activity, whereas AIRAP overexpression significantly increases resistance to the drug in melanoma cells. More importantly, during this study, we unexpectedly found that AIRAP-silencing hinders melanoma growth and promotes caspase activation and apoptosis of melanoma cells, also in the absence of pro-apoptotic stimuli. AIRAP-silencing for 48 hours was sufficient to trigger the cleavage of caspases-3, -7, -8, and -9, as well as PARP, promoting apoptosis in melanoma cells. In particular, AIRAP-silencing was found to be more effective than bortezomib in triggering caspase-8 cleavage. It should be noted that AIRAP silencing was shown not to affect human primary endothelial cell viability in the absence of stress (10), suggesting that loss of AIRAP would not impact the overall health of normal cells.

As indicated above, the AIRAP/ZFAND2A gene was initially described as a highly conserved gene, whose expression can be activated by arsenite and electrophiles in *C. elegans* and mammalian cells (1, 2). Differently from the AIRAP worm homologue

Published OnlineFirst September 20, 2019; DOI: 10.1158/1541-7786.MCR-19-0243

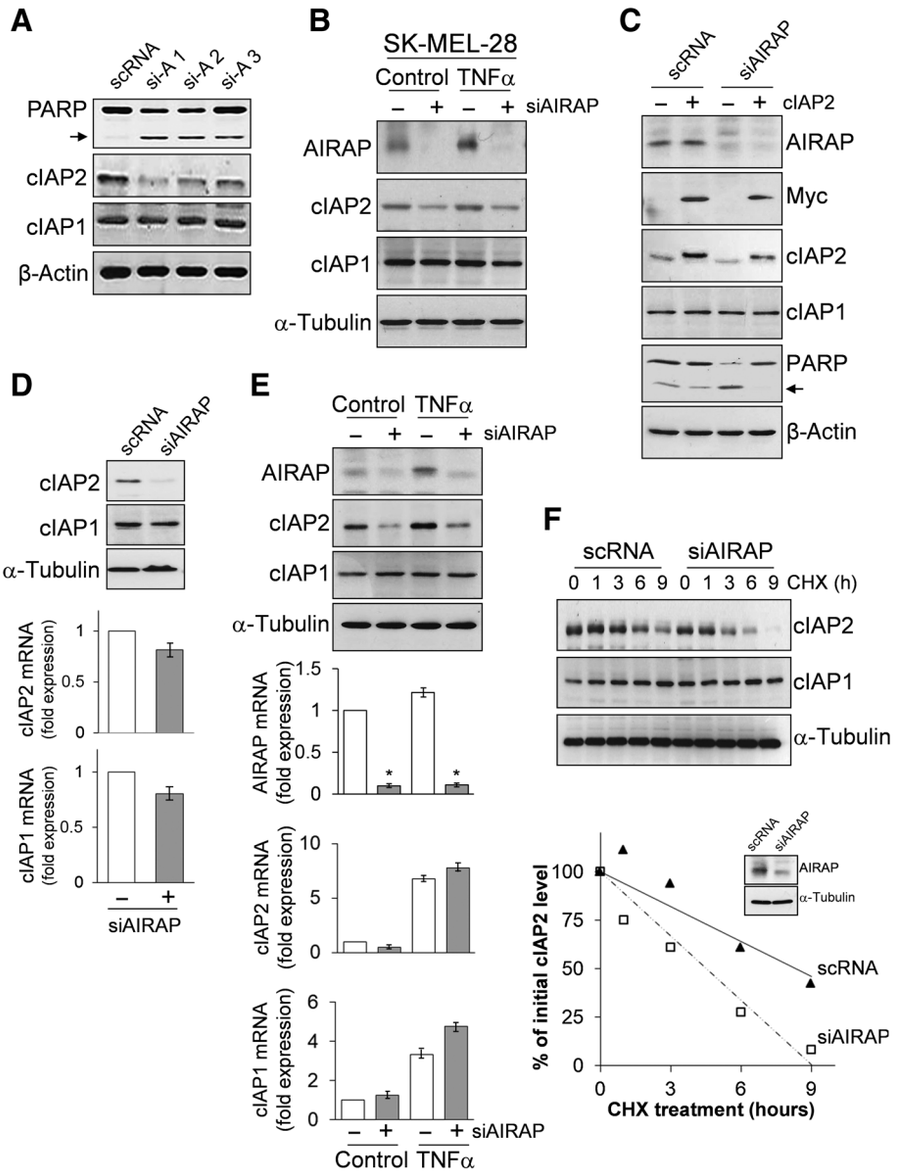

Figure 6.

AIRAP-knockdown affects cIAP2 protein stability in melanoma cells. **A,** M10 cells were transiently transfected with 3 different AIRAP-siRNAs: AIRAP-siRNA1 (si-A1), AIRAP-siRNA2 (si-A2), and AIRAP-siRNA3 (si-A3) or scramble-RNA (scRNA) and, after 60 hours, WCE were analyzed for levels of PARP, cIAP2, cIAP1, and β–actin by WB. Arrow indicates cleaved PARP fragments. **B,** SK-MEL-28 cells were transiently transfected with AIRAP-siRNA (siAIRAP) (+) or scramble-RNA (−) for 36 hours and then treated with TNFα (20 ng/mL) for 6 hours; WCE were analyzed for levels of AIRAP, cIAP2, cIAP1, and α-tubulin by WB. **C,** M10 cells were transiently transfected with siAIRAP or scRNA. After 12 hours, cells were transfected with pCMV3-Myc-BIRC3 (cIAP2) construct (+) or empty vector (−) for 48 hours and WCE were analyzed for levels of AIRAP, Myc, cIAP2, cIAP1, PARP, and β-actin by WB. Arrow indicates cleaved PARP fragments. **D,** M10 cells were transiently transfected with siAIRAP or scRNA and, after 72 hours, WCE were analyzed for levels of cIAP2, cIAP1, and α-tubulin by WB (top). In parallel samples, total RNA was analyzed for cIAP2, cIAP1, and β-actin expression by qRT-PCR (bottom). **E,** M10 cells transfected with siAIRAP (+) or scramble-RNA (−) for 36 hours were treated with TNFα (20 ng/mL) and, after 6 hours, WCE were analyzed for levels of AIRAP, cIAP2, cIAP1, and α-tubulin by WB (top). In parallel samples, total RNA was analyzed for AIRAP, cIAP2, cIAP1, and β-actin expression by qRT-PCR (bottom). **D** and **E,** Relative quantities of cIAP2, cIAP1, and AIRAP RNAs were normalized to β-actin. Fold expression was calculated by comparing the expression of the indicated genes in the treated samples to the relative control, which was arbitrarily set to 1. All reactions were made in duplicate using samples derived from at least 3 biological repeats. Error bars indicate ± SD. *, $P < 0.05$. **F,** M10 cells transfected with siAIRAP or scRNA for 36 hours were treated with TNFα (20 ng/mL). After 4.5 hours, TNFα was removed and cycloheximide CHX (100 μg/mL) was added (time 0); WCE were analyzed for levels of cIAP2, cIAP1, and α-tubulin at different times after CHX addition by WB (top). Relative amounts of cIAP2 protein were calculated after normalizing to α-tubulin (bottom). AIRAP levels at time 0 are shown (inset). Data from a representative experiment of 3 with similar results are shown.

Published OnlineFirst September 20, 2019; DOI: 10.1158/1541-7786.MCR-19-0243

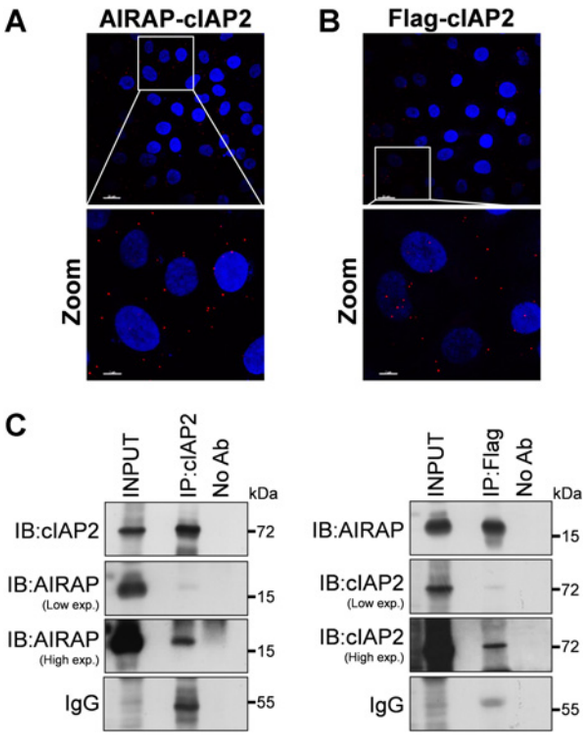

Figure 7.

AIRAP interacts with the antiapoptotic protein cIAP2 in M10 melanoma cells. **A** and **B,** AIRAP-cIAP2 and Flag-cIAP2 interactions (visualized as red spots) detected by *in situ* PLA in M10 cells (**A**) and in M10 cells expressing cFlag-tagged AIRAP (M10-AIRAP cells; **B**). Nuclei are stained with DAPI (blue). Scale bar, 20 μm (zoom, 7 μm). **C,** Co-IP of cIAP2 and AIRAP in M10 cells cotransfected with AIRAP-Flag and cIAP2-myc expression vectors. Cross-linked extracts were immunoprecipitated (IP) with anti-Flag or anti-cIAP2 antibodies and, after capture with protein-G-agarose beads, immunocomplexes were analyzed by Western blot (IB; see Materials and Methods, for detail). INPUT, negative control (No Ab), and IgG are shown. Data from a representative experiment of 3 with similar results are shown.

aip-1, a gene known to play an important role in preserving the animal lifespan and in buffering arsenic-induced proteotoxicity, mammals have a second, constitutively expressed, AIRAP-like gene, AIRAPL (3). There is no information on AIRAP function in cancer cells; however, AIRAPL was recently shown to cause myeloid transformation by deregulating insulin/insulin-like growth factor 1 (IGF-1) signaling (14). This observation prompted us to investigate whether AIRAP-silencing may affect AIRAPL expression in melanoma. AIRAP downregulation under conditions that caused caspase cleavage and cell death, did not cause changes in AIRAPL mRNA and protein levels, indicating that AIRAP functions independently of AIRAPL in melanoma.

Analysis of a panel of different antiapoptotic proteins implicated in caspase-cleavage control, led to the finding that AIRAP-silencing selectively affects the intracellular levels of cIAP2, an antiapoptotic protein stabilized in several cancer cells, and leading to bortezomib-resistance (23, 42). Among the numerous proteins and protein networks controlling the apoptotic pathways, inhibitor of apoptosis proteins (IAP) play an important role. IAPs are frequently overexpressed in various human cancers and their expression is associated with chemoresistance and poor clinical outcome (43, 44); consequently, IAPs have recently become attractive targets for cancer therapy, also in melanoma (22, 45, 46). In humans 8 IAPs have been identified so far including cIAP1, cIAP2, XIAP, NIAP, Apollon, Ts-IAP/ILP-2, survivin, and most recently the melanoma-associated ML-IAP/Livin. Most IAPs function as caspase-inhibitors, directly binding caspases via their BIR (baculoviral IAP-repeats)-domain(s) and adjacent sequences, whereas several IAPs possess ubiquitin-ligase activity (22, 45). In the case of cIAP2, this protein regulates caspase activation indirectly through its E3-ligase activity (22, 47, 48). In particular, cIAP2 and cIAP1 proteins are responsible for receptor-interacting protein 1 (RIP1) K63-linked polyubiquitination. In their absence, nonubiquitinated RIP1 can form a cytosolic complex with the adaptor molecule FADD and caspases-8, leading to induction of apoptosis (47–49). Therefore, we hypothesize that cIAP2 downregulation in AIRAP-silenced cells may trigger the apoptotic signal in melanoma cells; this hypothesis is supported by the fact that cIAP2 overexpression partially prevents the pro-apoptotic events following AIRAP-silencing. However, other mechanisms also involving the intrinsic pathway may participate in activating the AIRAP-dependent apoptotic signal, as suggested by caspase-9 cleavage in AIRAP-silenced cells. Moreover, the possibility that AIRAP may function as a pro-survival factor in other types of malignancies should also be considered, and is presently under investigation.

Regarding the mechanism leading to cIAP2 downregulation, we found that AIRAP-silencing does not alter cIAP2 mRNA expression both under normal conditions or after TNFα stimulation, whereas it affects cIAP2 protein stability; cIAP2 half-life is in fact significantly reduced (from 9 to 4.5 hours) in AIRAP-silenced melanoma cells. cIAP2 (but not cIAP1) stability was recently shown to be dependent on ubiquitin-specific protease-11 (USP11), a deubiquitylase frequently overexpressed in colorectal cancer and melanoma (24). Interestingly, AIRAP was found to interact with cIAP2, suggesting that this interaction is important for cIAP2 stability. AIRAP may interact with cIAP2 directly or it may be a component of a larger complex, including USP11, controlling melanoma cell survival via cIAP2 stabilization.

Altogether the results identify AIRAP/ZFAND2A as a novel HSF1-dependent prosurvival factor in melanoma cells. We also identify a novel survival axis involving HSF1/AIRAP/cIAP2, which may function to protect melanoma cells from bortezomib and other proapoptotic stimuli. On the basis of these observations, we propose AIRAP as a novel biomarker and therapeutic target in melanoma.

Disclosure of Potential Conflicts of Interest

No potential conflicts of interest were disclosed.

Authors' Contributions

Conception and design: S. Pizzato Scomazzon, A. Riccio, M.G. Santoro
Development of methodology: S. Pizzato Scomazzon, A. Riccio, S. Santopolo, A. Rossi, M. Coccia
Acquisition of data (provided animals, acquired and managed patients, provided facilities, etc.): S. Pizzato Scomazzon, A. Riccio, S. Santopolo, A. Rossi, G. Lanzilli, M. Coccia, M.G. Santoro
Analysis and interpretation of data (e.g., statistical analysis, biostatistics, computational analysis): S. Pizzato Scomazzon, A. Riccio, S. Santopolo, A. Rossi, M.G. Santoro

Writing, review, and/or revision of the manuscript: S. Pizzato Scomazzon, A. Riccio, S. Santopolo, M.G. Santoro
Administrative, technical, or material support (i.e., reporting or organizing data, constructing databases): S. Pizzato Scomazzon, A. Riccio, S. Santopolo, A. Rossi, G. Lanzilli, M. Coccia, M.G. Santoro
Study supervision: M.G. Santoro

Acknowledgments

The authors thank G. Zupi (Regina Elena Cancer Institute, Rome, Italy) for providing the M10 melanoma cell line, and E. Romano (Center for Advanced Microscopy, University of Rome Tor Vergata) for assistance with confocal microscopy. This work was supported by grants from the Italian Ministry of University and Scientific Research (PRIN project N 2010PHT9NF-006). S. Pizzato Scomazzon is recipient of a scholarship from CAPES, Brazil.

The costs of publication of this article were defrayed in part by the payment of page charges. This article must therefore be hereby marked *advertisement* in accordance with 18 U.S.C. Section 1734 solely to indicate this fact.

Received March 8, 2019; revised June 13, 2019; accepted September 17, 2019; published first September 20, 2019.

References

1. Sok J, Calfon M, Lu J, Lichtlen P, Clark SG, Ron D. Arsenite-inducible RNA-associated protein (AIRAP) protects cells from arsenite toxicity. Cell Stress Chaperones 2001;6:6–15.
2. Stanhill A, Haynes CM, Zhang Y, Min G, Steele MC, Kalinina J, et al. An arsenite-inducible 19S regulatory particle-associated protein adapts proteasomes to proteotoxicity. Mol Cell 2006;23:875–85.
3. Yun C, Stanhill A, Yang Y, Zhang Y, Haynes CM, Xu CF, et al. Proteasomal adaptation to environmental stress links resistance to proteotoxicity with longevity in Caenorhabditis elegans. Proc Natl Acad Sci U S A 2008;105:7094–9.
4. Rossi A, Trotta E, Brandi R, Arisi I, Coccia M, Santoro MG. AIRAP, a new human heat shock gene regulated by heat shock factor 1. J Biol Chem 2010;285:13607–15.
5. Gomez-Pastor R, Burchfiel ET, Thiele DJ. Regulation of heat shock transcription factors and their roles in physiology and disease. Nat Rev Mol Cell Biol 2018;19:4–19.
6. Akerfelt M, Morimoto RI, Sistonen L. Heat shock factors: integrators of cell stress, development and lifespan. Nat Rev Mol Cell Biol 2010;11:545–55.
7. Trinklein ND, Murray JI, Hartman SJ, Botstein D, Myers RM. The role of heat shock transcription factor 1 in the genome-wide regulation of the mammalian heat shock response. Mol Biol Cell 2004;15:1254–61.
8. Vihervaara A, Sergelius C, Vasara J, Blom MA, Elsing AN, Roos-Mattjus P, et al. Transcriptional response to stress in the dynamic chromatin environment of cycling and mitotic cells. Proc Natl Acad Sci U S A 2013;110:3388–97.
9. Coccia M, Rossi A, Riccio A, Trotta E, Santoro MG. Human NF-κB repressing factor acts as a stress-regulated switch for ribosomal RNA processing and nucleolar homeostasis surveillance. Proc Natl Acad Sci U S A 2017;114:1045–50.
10. Rossi A, Riccio A, Coccia M, Trotta E, La Frazia S, Santoro MG. The proteasome inhibitor bortezomib is a potent inducer of zinc finger AN1-type domain 2a gene expression: role of heat shock factor 1 (HSF1)-heat shock factor 2 (HSF2) heterocomplexes. J Biol Chem 2014;289:12705–15.
11. Chen D, Frezza M, Schmitt S, Kanwar J, Dou QP. Bortezomib as the first proteasome inhibitor anticancer drug: current status and future perspectives. Curr Cancer Drug Targets 2011;11:239–53.
12. Ferrarini M, Ferrero E. Proteasome inhibitors and modulators of angiogenesis in multiple myeloma. Curr Med Chem 2011;18:5185–95.
13. Shahshahan MA, Beckley MN, Jazirehi AR. Potential usage of proteasome inhibitor bortezomib (Velcade, PS-341) in the treatment of metastatic melanoma: basic and clinical aspects. Am J Cancer Res 2011;1:913–24.
14. Osorio FG, Soria-Valles C, Santiago-Fernández O, Bernal T, Mittelbrunn M, Colado E, et al. Loss of the proteostasis factor AIRAPL causes myeloid transformation by deregulating IGF-1 signaling. Nat Med 2016;22:91–6.
15. Selimovic D, Porzig BBOW, El-Khattouti A, Badura HE, Ahmad M, Ghanjati F, et al. Bortezomib/proteasome inhibitor triggers both apoptosis and autophagy-dependent pathways in melanoma cells. Cell Signal 2013;25:308–18.
16. Golub SH, Hanson DC, Sulit HL, Morton DL, Pellegrino MA, Ferrone S. Comparison of histocompatibility antigens on cultured human tumor cells and fibroblasts by quantitative antibody absorption and sensitivity to cell-mediated cytotoxicity. J Natl Cancer Inst 1976;56:167–70.
17. Rossi A, Kapahi P, Natoli G, Takahashi T, Chen Y, Karin M, et al. Anti-inflammatory cyclopentenone prostaglandins are direct inhibitors of IκB kinase. Nature 2000;403:103–8.
18. Rossi A, Elia G, Santoro MG. Inhibition of nuclear factor κB by prostaglandin A_1: an effect associated with heat shock transcription factor activation. Proc Natl Acad Sci U S A 1997;94:746–50.
19. Franken NA, Rodermond HM, Stap J, Haveman J, van Bree C. Clonogenic assay of cells in vitro. Nat Protoc 2006;1:2315–9.
20. Andersen AP, Flinck M, Oernbo EK, Pedersen NB, Viuff BM, Pedersen SF. Roles of acid-extruding ion transporters in regulation of breast cancer cell growth in a 3-dimensional microenvironment. Mol Cancer 2016;15:45.
21. Zanoni M, Piccinini F, Arienti C, Zamagni A, Santi S, Polico R, et al. 3D tumor spheroid models for in vitro therapeutic screening: a systematic approach to enhance the biological relevance of data obtained. Sci Rep 2016;6:19103.
22. Fulda S, Vucic D. Targeting IAP proteins for therapeutic intervention in cancer. Nat Rev Drug Discov 2012;11:109–24.
23. Petersen SL, Peyton M, Minna JD, Wang X. Overcoming cancer cell resistance to Smac mimetic induced apoptosis by modulating cIAP-2 expression. Proc Natl Acad Sci U S A 2010;107:11936–41.
24. Lee EW, Seong D, Seo J, Jeong M, Lee HK, Song J. USP11-dependent selective cIAP2 deubiquitylation and stabilization determine sensitivity to Smac mimetics. Cell Death Differ 2015;22:1463–76.
25. Eggermont AMM, Robert C, Ribas A. The new era of adjuvant therapies for melanoma. Nat Rev Clin Oncol 2018;15:535–6.
26. Fattore L, Costantini S, Malpicci D, Ruggiero CF, Ascierto PA, Croce CM, et al. MicroRNAs in melanoma development and resistance to target therapy. Oncotarget 2017;8:22262–78.
27. Hutchinson L. Skin cancer. Golden age of melanoma therapy. Nat Rev Clin Oncol 2015;12:1.
28. Robert C, Long GV, Brady B, Dutriaux C, Maio M, Mortier L, et al. Nivolumab in previously untreated melanoma without BRAF mutation. N Engl J Med 2015;372:320–30.
29. Soengas MS, Lowe SW. Apoptosis and melanoma chemoresistance. Oncogene 2003;22:3138–51.
30. Manasanch EE, Orlowski RZ. Proteasome inhibitors in cancer therapy. Nat Rev Clin Oncol 2017;14:417–33.
31. Reuland SN, Goldstein NB, Partyka KA, Smith S, Luo Y, Fujita M, et al. ABT-737 synergizes with Bortezomib to kill melanoma cells. Biol Open 2012;1:92–100.
32. Li J, Labbadia J, Morimoto RI. Rethinking HSF1 in stress, development, and organismal health. Trends Cell Biol 2017;27:895–905.
33. Dai C, Sampson SB. HSF1: guardian of proteostasis in cancer. Trends Cell Biol 2016;26:17–28.
34. Min JN, Huang L, Zimonjic DB, Moskophidis D, Mivechi NF. Selective suppression of lymphomas by functional loss of Hsf1 in a p53-deficient mouse model for spontaneous tumors. Oncogene 2007;26:5086–97.
35. Rossi A, Ciafrè S, Balsamo M, Pierimarchi P, Santoro MG. Targeting the heat shock factor 1 by RNA interference: a potent tool to enhance hyperthermochemotherapy efficacy in cervical cancer. Cancer Res 2006;66:7678–85.
36. Ciocca DR, Arrigo AP, Calderwood SK. Heat shock proteins and heat shock factor 1 in carcinogenesis and tumor development: an update. Arch Toxicol 2013;87:19–48.
37. Chou SD, Murshid A, Eguchi T, Gong J, Calderwood SK. HSF1 regulation of β-catenin in mammary cancer cells through control of HuR/elavL1 expression. Oncogene 2015;34:2178–88.
38. Su KH, Cao J, Tang Z, Dai S, He Y, Sampson SB, et al. HSF1 critically attunes proteotoxic stress sensing by mTORC1 to combat stress and promote growth. Nat Cell Biol 2016;18:527–39.

Published OnlineFirst September 20, 2019; DOI: 10.1158/1541-7786.MCR-19-0243

39. Santagata S, Hu R, Lin NU, Mendillo ML, Collins LC, Hankinson SE, et al. High levels of nuclear heat-shock factor 1 (HSF1) are associated with poor prognosis in breast cancer. Proc Natl Acad Sci U S A 2011; 108:18378–83.
40. Mendillo ML, Santagata S, Koeva M, Bell GW, Hu R, Tamimi RM, et al. HSF1 drives a transcriptional program distinct from heat shock to support highly malignant human cancers. Cell 2012;150:549–62.
41. Kourtis N, Moubarak RS, Aranda-Orgilles B, Lui K, Aydin IT, Trimarchi T, et al. FBXW7 modulates cellular stress response and metastatic potential through HSF1 post-translational modification. Nat Cell Biol 2015;17: 322–32.
42. Fristedt Duvefelt C, Lub S, Agarwal P, Arngården L, Hammarberg A, Maes K, et al. Increased resistance to proteasome inhibitors in multiple myeloma mediated by cIAP2-implications for a combinatorial treatment. Oncotarget 2015;6:20621–35.
43. Gyrd-Hansen M, Meier P. IAPs: from caspase inhibitors to modulators of NF-κB, inflammation and cancer. Nat Rev Cancer 2010;10:561–74.
44. Chen N, Gong J, Chen X, Meng W, Huang Y, Zhao F, et al. Caspases and inhibitor of apoptosis proteins in cutaneous and mucosal melanoma: expression profile and clinicopathologic significance. Hum Pathol 2009; 40:950–6.
45. LaCasse EC, Mahoney DJ, Cheung HH, Plenchette S, Baird S, Korneluk RG. IAP-targeted therapies for cancer. Oncogene 2008; 27:6252–75.
46. Hartman ML, Czyz M. Anti-apoptotic proteins on guard of melanoma cell survival. Cancer Lett 2013;331:24–34.
47. Vaux DL, Silke J. IAPs, RINGs and ubiquitylation. Nat Rev Mol Cell Biol 2005;6:287–97.
48. Bertrand MJ, Milutinovic S, Dickson KM, Ho WC, Boudreault A, Durkin J, et al. cIAP1 and cIAP2 facilitate cancer cell survival by functioning as E3 ligases that promote RIP1 ubiquitination. Mol Cell 2008;30: 689–700.
49. Liu XY, Lai F, Yan XG, Jiang CC, Guo ST, Wang CY, et al. RIP1 kinase is an oncogenic driver in melanoma. Cancer Res 2015;75:1736–48.

Published OnlineFirst September 20, 2019; DOI: 10.1158/1541-7786.MCR-19-0243

Molecular Cancer Research

The Zinc-Finger AN1-Type Domain 2a Gene Acts as a Regulator of Cell Survival in Human Melanoma: Role of E3-Ligase cIAP2

Sofia Pizzato Scomazzon, Anna Riccio, Silvia Santopolo, et al.

Mol Cancer Res 2019;17:2444-2456. Published OnlineFirst September 20, 2019.